# Physicochemical and biological controls on primary and net community production across northeast Pacific seascapes

Maria T. Kavanaugh,[1,*] Steven R. Emerson,[2] Burke Hales,[3] Deirdre M. Lockwood,[2] Paul D. Quay,[2] and Ricardo M. Letelier[3]

[1] Department of Marine Chemistry and Geochemistry, Woods Hole Oceanographic Institution, Woods Hole, Massachusetts
[2] Department of Oceanography, University of Washington, Seattle, Washington
[3] College of Earth, Ocean and Atmospheric Sciences, Oregon State University, Corvallis, Oregon

*Abstract*

The subarctic–subtropical transition zone in the North Pacific represents the second largest sink of atmospheric carbon dioxide in the world ocean, yet the relative importance of physical and biological processes in this uptake is debated. In a step toward understanding the spatiotemporal variability of environmental, physiological, and ecological factors that contribute to the efficacy of the biological pump, near-continuous measurements of net primary production (NPP), net community production (NCP), export efficiency (NCP : NPP), and several physiological and ecological variables were collected across subarctic, transition, and subtropical seascapes of the Northeast Pacific during August and September of 2008. Whereas hydrographic variability (e.g., temperature, salinity, and mixed layer) dominated at basin scales, the effects were balanced or subsumed by biomass or taxa effects within individual seascapes. Fluorescence diagnostics suggested that the transition seascape was neither iron nor macronutrient limited. NPP and NCP were strongly spatially coupled in both the transition ($r = 0.70$; $p < 0.0001$) and subtropics ($r = 0.68$, $p < 0.0001$); however, the strength of individual drivers as determined through multiple linear regression (MLR) varied across seascapes. NPP in the transition seascape was driven primarily by nano- and microphytoplankton biomass, whereas NCP appeared to be driven by changes in salinity, temperature, and to a lesser degree, diatom-specific biomass. Although NPP was low in the subtropics, mesoscale changes in hydrographical factors and shifts in community structure from pico- to microphytoplankton contributed to moderate NCP and high export efficiency. Spatial variability in the relative importance of hydrography, phytoplankton community structure, and NPP in driving NCP illuminates regional sensitivity of the biological pump to future climate conditions.

The ocean carbon cycle modulates global climate by acting as a sink for atmospheric carbon dioxide (Siegenthaler and Sarmiento 1993), but climate also affects the magnitude of the ocean's carbon sink by altering the functioning of the biological and solubility pumps (Emerson et al.1997; Monahan and Denman 2004). Although we have been able to characterize the location of carbon source and sink regions of the ocean and how they change on a seasonal basis (Takahashi et al. 2002, 2009), our understanding of future changes in the efficiency of biological carbon sequestration is still rudimentary. In general, biological systems will respond to perturbations by adjusting bulk processes, such as primary production and respiration rates, and through shifts in ecosystem structure (Falkowski et al. 1998). However, predicting the effects of global change on the ocean is problematic because ecosystems evolve nonlinearly at both the physiological and community levels as organisms respond to gradients and patches in the environment. Thus, accurate monitoring of the biological pump in conjunction with high-resolution measurements of physiological and taxonomic diversity can help us to understand how the oceans will modulate, and in turn be affected by, future climate trends.

The decoupling between production and remineralization that controls the efficiency of the biological pump represents an interaction between environmental variability

and the evolutionary drive to optimize energy use and limited resources (Margalef 1968). Net primary production (NPP) is governed primarily by the availability of light and nutrients, and describes the difference between gross primary production (GPP) and autotrophic respiration. The difference between NPP and local heterotrophic respiration of organic matter is termed "net community production" (NCP; Williams 1998). At steady state and when averaged over sufficient length scales, NCP should be equivalent to export production (Laws et al. 2000), i.e., the flux of organic carbon out of the euphotic zone driven by the biological pump. This export takes place by sinking or advection of particulate and dissolved organic matter or via zooplankton migration. However, the "efficiency" of the biological pump, or the fraction that reaches the deep sea, is controlled by numerous processes including aggregation of organic particles, microbial remineralization, grazing and fecal pellet production, and interactions between organic aggregates and ballast minerals such as $CaCO_3$ and $SiO_2$ (Brix et al. 2006; De La Rocha and Passow 2007). Understanding these processes and their relevant time- and space scales will provide insight into ecosystem resilience and the maintenance of the biological pump under the stress of environmental change.

Both physiological and ecological interactions within the phytoplankton community can affect the magnitude and efficiency of the biological pump; thus a mechanistic understanding of the spatiotemporal variability of the

* Corresponding author: mkavanaugh@whoi.edu

relationships between GPP or NPP and NCP remains elusive. Ecosystem or empirical models that attempt to obtain these relationships from satellite-derived chlorophyll *a* (Chl *a*) and sea-surface temperature (SST; Laws et al. 2000; Dunne et al. 2005) perform reasonably well globally but are limited in their capacity to predict organic carbon export at local to gyre scales. Spatial variability of nutrient supply, particularly iron (Mahowald et al. 2009), can affect phytoplankton responses to light and temperature (Maldonado et al. 1999; Boyd et al. 2004) as well as local community structure. Regional shifts in community structure can likewise impart variability in the relationship of primary to export production. For example, Serret et al. (2002) found that the threshold GPP necessary to support net autotrophy (positive NCP) suggested by meta-analysis (Duarte and Regaudie de Gioux 2009) and theoretical studies (Lopez-Urrutia et al. 2006) had poor predictive capacity outside of the subtropics primarily due to a failure to account for different species effects. Thus, to understand how the biological pump may modulate or respond to different climate scenarios, we must account for regional differences in physiology and community structure in an objective and spatially explicit fashion.

The subarctic–subtropical transition zone from the Kuroshio extension into the eastern subarctic gyre is the largest sink region for atmospheric carbon dioxide in the North Pacific (Takahashi et al. 2009) and the second largest ocean sink on the planet. Until recently, it was thought that although biological uptake of dissolved inorganic carbon (DIC) counteracted the warming effect on $CO_2$ solubility in the summer, the bulk of the drawdown was due to winter cooling and the resultant increase in solubility of $CO_2$ in seawater (Takahashi et al. 2002). More recent estimates of NCP across the eastern transition zone suggest that during the spring–summer growing season the effect of biological drawdown is as, or more, important than the effect of solubility (Howard et al. 2010; Juranek et al. 2012; Lockwood et al. 2012), in terms of both spatial and temporal drivers of $P_{CO_2}$. However, how the biological pump is primed in this geochemically important region, in terms of carbon assimilation and mechanisms driving the subsequent export, is not understood. This uncertainty highlights the importance of consistent measurements of both NPP and NCP and a mechanistic understanding of the spatiotemporal variability in the physiological and ecological effects on NPP, NCP, and the ratio between them.

Over the course of a 3-week cruise spanning the eastern subarctic, transition, and subtropical Pacific, we measured NPP, NCP, and several physical, physiological, and ecological variables at very high resolution (minutes to days). Thus, we were able to obtain a data set that allowed evaluation of local (including diurnal variability) to basin-scale drivers of both NPP and NCP. Previous studies indicated that biogeochemical patterns and biophysical forcing of $P_{CO_2}$ were different across seasonally dynamic seascapes (Kavanaugh et al. 2014). Here, we apply a similar approach to the analysis of spatial data to understand the relative effect of hydrography, phytoplankton community structure, NPP, and particle export efficiency on NCP in the upper ocean. Specifically, we address the following questions: (1) How do these factors vary in space, both continuously and as a function of objectively defined seascapes? (2) How does the spatial relationship of NPP : NCP change as a function of seascape? and finally, (3) What is the relative importance of physical and physiological or ecological variability in driving both NPP and NCP within and across seascapes?

## Methods

*Regional analysis*—Distinct seascapes were determined a priori on the basis of the biophysical climatology described in Kavanaugh et al. (2014). In brief, seascapes were classified by a combination of a probabilistic self-organizing map and a hierarchical clustering algorithm. This method maintains underlying biophysical distributions of Chl *a* (from the sea-viewing wide field-of-view sensor, SeaWIFs), SST (from the advanced very-high-resolution radiometer), and photosynthetically active radiation (PAR from SeaWiFs), resulting in objectively defined, distinct water masses (Kavanaugh et al. 2014). We present divisions in the August and September 2008 ship tracks on the basis of the climatological location of boundaries in August (based on the preceding 10 yr: 1998–2007). Four seascapes were sampled over four transects of the cruise (Fig. 1). These included a summer subarctic seascape (SuSA), characterized by cooler temperatures and high Chl *a*; a summer transition seascape (SuTR) that identifies the region between the subarctic and subtropical fronts, bounded in the south by the approximate position of the transition-zone chlorophyll front ((TZCF; Polovina et al. 2001); an oligotrophic boundary seascape (OB) that has moderately low Chl *a* (Kavanaugh et al. 2014); and a summer subtropical seascape that has persistently low Chl *a* (SuST, $< 0.07$ $\mu g$ $L^{-1}$). The ship's track crossed through all four seascapes, with longitudinal repeat transects in the SuSA, SuTR, and OB seascapes (Fig. 1). The first leg followed a direct route from the Strait of Juan de Fuca to Ocean Station Papa (50°N, 145°W). The second leg consisted of a southward track along 145°W through the SuTR to approximately 38°N. The third leg consisted of a diagonal across the transition from 38°N, 145°W to 48°N, 152°W. The final leg traveled along 152°W, which crossed the transition a third time, traveling due south along 152°W through the OB and SuST seascapes toward the Hawaiian Islands. Stations were sampled approximately every degree; however, high-resolution sampling from the ship's flow-through system occurred nearly continuously.

*Ancillary measurements*—SST, PAR, salinity, and $P_{CO_2}$ were collected as part of the ship's flow-through system. Underway $P_{CO_2}$ was measured from surface water and air from the ship's bow with an automated infrared detection system described in detail elsewhere (Feely et al. 1998; Lockwood et al. 2012 and references therein). Nutrients were collected at discrete stations and depths (Lockwood et al. 2012); only surface values ($\sim 5$ m) are reported here. Sea-surface height (SSH) deviations were downloaded from National Oceanic and Atmospheric Administration
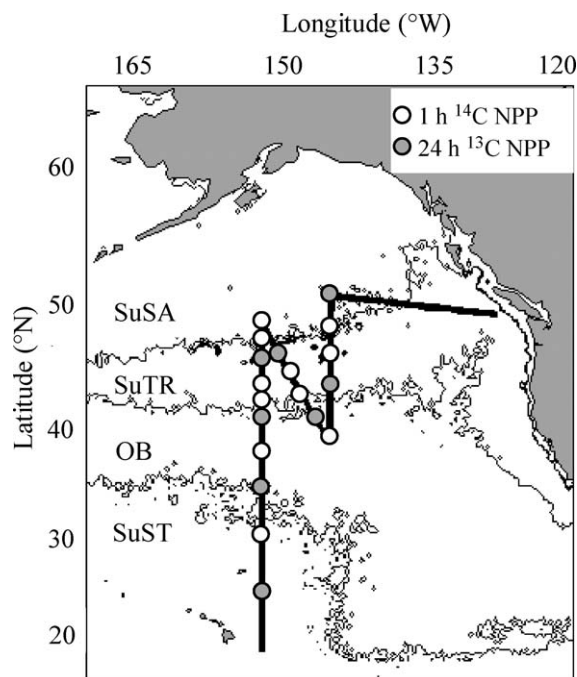
Fig. 1. Cruise track across Northeast Pacific seascapes. Seascape boundaries (thin black contours) demarcate four objectively determined seascapes classified from monthly climatologies (1998–2007) of satellite-derived Chl *a*, SST, and PAR for August. SuSA = summer subarctic; SuTR = summer transition; OB = oligotrophic boundary; and SuST = summer subtropical. Gray circles denote stations where $^{13}$C incubations were conducted in addition to $^{14}$C incubations (open circles; *see* Methods).

Coastwatch page (*http://oceanwatch.pifsc.noaa.gov/*) at 8-d and 1/3° resolution and matched to the cruise track.

*Community structure and dominant size classes*—To understand how changes in the assemblage affect NPP and NCP, we measured phytoplankton pigment diversity and derived size classes from high-performance liquid chromatography (HPLC). Photosynthetic or accessory pigments were determined using a C8 column according to Goericke and Repeta (1992). The relative biomass of prochlorophytes vs. all other phytoplankton was assessed using the spatial patterns of divinyl (DV) Chl *a* and monovinyl (MV) Chl *a*. Pigment diversity was assessed using the Shannon–Weiner diversity index (*H*′) on HPLC-derived pigment concentrations, specifically:

$$H' = \sum_i^h p_i \ln(p_i) \qquad (1)$$

where $p_i$ is the fraction of the *i*th pigment to total pigment concentration in a sample and *H*′ is the sum across all *h* pigments in a sample, where maximum possible *h* was 26.

Size classes were derived from HPLC pigments using the methods described by Bricaud et al. (2004) and Uitz et al. (2006) that utilize a MLR model to characterize percent contribution of each size class to total Chl *a*. In brief, the ratios of pigments diagnostic for picophytoplankton

(zeaxanthin, Chl *b*, and DV Chl *b*), nanophytoplankton (alloxanthin and 19-hexanoyl fucoxanthin [19-HEX]), and microphytoplankton (fucoxanthin [FUCO] and peridinium) to total Chl *a* are used to determine the percent contribution of pico-, nano-, and microphytoplankton to total Chl *a*. The ratios of accessory pigments to total Chl *a* have been empirically determined, are valid for the size classes of natural populations in case 1 waters, and have been tested at local and global (Uitz et al. 2006) scales. For our study, size class contributions determined with this method agreed well with biomass estimates on the basis of cell counts (flow cytometry), explaining 69%, 71%, or 77% of the variability of pico-, nano-, and microphytoplankton, respectively (M. Kavanaugh unpubl. data). Total biomass for each class was calculated by multiplying percent contribution by total Chl *a*.

The relative biomass of diatoms to haptophytes (including coccolithophores) was estimated using the ratio of FUCO and its derivative 19-HEX. We acknowledge the debate regarding the common usage of 19-HEX to indicate oceanic coccolithophores because of its occurrence across multiple coccolith- and noncoccolith-forming taxa (Van Lenning et al. 2004). However, recent investigations have found good agreement of 19-HEX concentrations with coccolithophore biovolume (Dandonneau et al. 2006).

*Primary production and fast repetition rate fluorometry*— Primary productivity was measured using 1 h $^{14}$C incubations and 24 h $^{13}$C incubations at several stations across the cruise track (Fig. 1). At just after dawn, surface samples (5 m) were collected from the rosette or from the underway system. Photosynthesis vs. irradiance (P vs. E) curves were derived from $^{14}$C uptake measurements after 1 h incubations of 10 mL subsamples in temperature-controlled photosynthetrons, modified from the design of Jassby and Platt (1976). A total of 24 subsamples was incubated across a light gradient in the photosynthetrons; irradiance varied from ~ 20 to ~ 700 $\mu$E m$^{-2}$ s$^{-1}$. The maximal C-assimilation rate ($P_{max}$) was determined through nonlinear least-squares fit (MATLAB®: *nlfit*) of the hyperbolic tangent approximation to the P vs. E curves (Jassby and Platt 1976) with least-squares parameter estimates and confidence intervals using the Gauss–Newton algorithm with Levenberg–Marquardt modifications for global convergence.

The $^{13}$C experiments were conducted on the same surface seawater as the $^{14}$C experiments, using 2 liter volumes (*n* = 3) collected just before dawn, supplemented with 99% $^{13}$C-bicarbonate solution and incubated for 24 h in seawater-cooled incubators located on the ship's deck. The $^{13}$C experiments were conducted on the same surface water as the $^{14}$C experiments, using 2 liter volumes (*n* = 3) collected just before dawn, supplemented with 99% $^{13}$C-bicarbonate solution, and incubated for 24 h in seawater-cooled incubators located on the ship's deck. C-assimilation rate was calculated as the change in $^{13}$C : $^{12}$C in the particulate organic carbon (POC) pool following Hama et al. (1983).

Fast repetition rate fluorometry (FRRf) was used as a diagnostic of nutrient stress (Behrenfeld et al. 2006) as well as a means of spatially interpolating between discrete

Table 1. Surface NPP comparing ^{14}C and ^{13}C incubations across the Northeast Pacific. NPP for both experiments is reported in mg C m$^{-3}$ d$^{-1}$. Mean ($\pm$ SD) was assessed through the parameterization of the light response curve for ^{14}C incubations and across replicates ($n = 3$) for the ^{13}C incubations (*see* Methods). Mean ratio was 1.02 ($\pm$ 0.2).

| Latitude (°N) | Longitude (°W) | $P_{max}$ (mg C m$^{-3}$ h$^{-1}$) | Day length (h) | ^{14}C-NPP | ^{13}C-NPP | ^{14}C-NPP : ^{13}C-NPP |
|---|---|---|---|---|---|---|
| 50 | −145 | 3.25 | 13.45 | 43.72 (2.94) | 38.31 (20.61) | 1.14 |
| 47.2 | −145 | 2.17 | 13.31 | 28.9 (1.62) | | |
| 46 | −145 | 6.27 | 13.26 | 83.16 (4.62) | | |
| 44 | −145 | | 13.17 | | 40.72 (3.36) | |
| 39.2 | −145 | 0.62 | 13 | 8.06 (0.65) | | |
| 40 | −146.5 | 0.89 | 13.02 | 11.58 (1.13) | 8.37 (0.91) | 1.38 |
| 43 | −148 | 0.87 | 13.14 | 11.42 (3.29) | | |
| 44 | −148.5 | 0.83 | 13.17 | 10.95 (1.88) | | |
| 47.3 | −152 | 2.06 | 13.32 | 27.5 (1.24) | | |
| 47 | −152 | 1.56 | 13.31 | 20.76 (1.45) | | |
| 46 | −152 | 2.93 | 13.26 | 38.83 (1.67) | 43.64 (6.98) | 0.89 |
| 46 | −151 | 3.19 | 13.26 | 42.36 (1.98) | 47.39 (2.99) | 0.89 |
| 44 | −152 | 1.28 | 13.17 | 16.92 (1.00) | | |
| 43 | −152 | 1.52 | 13.04 | 19.95 (1.75) | | |
| 42 | −152 | 0.81 | 13.09 | 10.60 (9.55) | 10.14 (0.75) | 1.04 |
| 38 | −152 | 0.97 | 12.95 | 12.52 (1.35) | | |
| 34 | −152 | 0.65 | 12.82 | 8.32 (1.13) | 10.47 (1.25) | 0.8 |
| 30 | −152 | 0.76 | 12.7 | 9.71 (8.00) | | |
| 24 | −152 | 0.84 | 12.54 | 10.49 (0.81) | 10.37 (1.21) | 1.01 |

primary productivity measurements (Kolber et al. 1998). The FRRf uses rapid flashlets to saturate the photosystems, allowing both the determination of the quantum yield of fluorescence (Fv : Fm) and the functional cross-section of photosystem II ($\sigma_{PSII}$, from the slope of the saturation curve). On broad scales, low values of Fv : Fm are associated with communities acclimated to chronic Fe limitation and excess nitrogen (Behrenfeld et al. 2006), although the responses also are taxa specific (Suggett et al. 2009). The FRRf was installed on the ship's flow-through system, allowing near-continuous measurement of Fv : Fm and $\sigma_{PSII}$. Diurnal patterns of Fv : Fm were compared across seascapes by binning measurements to the nearest hour and averaging across days within seascapes.

In theory, the FRRf measures the light reactions and approximates gross oxygen evolution, a measurement of GPP (Kolber et al. 1998). Thus, the FRRf provides a means of interpolating GPP in space and over relatively short timescales (e.g., Corno et al. 2006; Suggett et al. 2009). However, the ^{14}C rates used for tuning, when scaled to day length, were equivalent to ^{13}C NPP measurements (Table 1). The similarity across water types suggested that the ^{14}C measurements approximated NPP rather than GPP as found for other short-term incubation (Marra 2009; Halsey et al. 2010). We therefore derived a spatially variable NPP proxy (NPPp) on the basis of the product of the FRRf-derived parameters, Chl $a$, and mean daily PAR. Specifically,

$$NPPp = m(Fv:Fm \times \sigma_{PSII} \times [Chl\ a] \times PAR \times c_1) + c_2 \quad (2)$$

Here, surface Chl $a$ was determined through spatial interpolation of Fm ([Chl $a$] = 0.001031 × Fm; $R^2$ = 0.81, $p < 0.0001$, $n = 72$); $c_1$ is a constant (Corno et al. 2006) that includes conversions for photon flux, rate unit (seconds to hours), an assumption of four photons required for each molecule of oxygen evolved, and a fixed number of

reaction centers based on typical prokaryotic-dominated primary production. The parameters $m$ and $c_2$ were determined by linear regression between the FRRf-based NPP and maximum primary productivity determined from ^{14}C incubations ($P_{max}$; Table 1), which allowed for variation in the dominance of prokaryotes to eukaryotes on the basis of the relative concentration of DV Chl $a$ to Chl $a$. Differences in slope for prokaryotic vs. eukaryotic regions (Table 2) are likely a result of keeping the number of reaction centers fixed. PAR was measured using a biospherical PAR sensor deployed on a gimbaled mast in a nonshaded region of the ship. Because we were interested in the spatial variability in NPPp, diurnal variations in FRRf-derived properties were removed for this calculation using a medium loess-smoothing filter (6–26 h) before spatial tuning. Spatial tuning of both the Fm : Chl $a$ relationship and the FRRf : [14]C relationship was then conducted using least-squares regression to the nearest cast or underway water grab, with error assessed over $\pm$ 15 min.

*NCP and export efficiency*—NCP was calculated via equilibrator inlet mass spectrometry (EIMS) from the balance of net $O_2$ production in the water and loss to the atmosphere by gas exchange. Detailed methodology is given in Lockwood et al. (2012). Briefly, a gear pump continuously draws water from the ship's seawater supply line through an equilibrator cartridge, and gases from the equilibrator are introduced into a quadrupole mass spectrometer (Pfeiffer Prisma quadrupole mass spectrometer; Cassar et al. 2009; Lockwood et al. 2012). The measured $O_2$ : Ar ion current ratio is normalized to the $O_2$ : Ar ratio of air measured by the EIMS. The EIMS-based $O_2$ : Ar measurements are further calibrated with high-precision isotope ratio mass spectrometer $O_2$ : Ar measurements of discrete samples taken along the ship's track (Howard et al. 2010; Lockwood et al. 2012). In this

Table 2. Regression models used to spatially tune the NPPp from the FRRf $^{14}$C relationship. *F*-statistics and degrees of freedom (df) for each regression model shown for the entire region and each subregion. Unique lowercase letters denote statistically distinct slopes as determined by a two-sided *t*-test. Northern vs. southern subregion *t*-statistic = 2.782, *p* = 0.036.

| Scale | *F*-statistic (df) | *p* | Intercept (SE) | Slope (SE) | $R^2$ |
|---|---|---|---|---|---|
| Northeast Pacific | 115.0 (1/16) | <0.0001 | 0.292 (0.193) | 1.062 (0.099)a | 0.88 |
| >42.5°N | 55.1 (1/10) | <0.0001 | 0.211 (0.340) | 1.088 (0.151)a | 0.85 |
| <42°N | 17.1 (1/5) | 0.0256 | 0.530 (0.314) | 3.398 (0.821)b | 0.81 |

method, normalization by Ar removes the influence of nonbiological processes such as warming and bubble injection on $O_2$ saturation to derive an estimate of biological $O_2$ saturation ($O_2$-sat $_{BIO}$; Emerson et al. 1997). These measurements are reported in terms of saturation (%) − 100%, where $O_2$-sat $_{BIO}$ > 0 suggests net autotrophy over the timescale of the measurement.

Combining EIMS measurement of percent $O_2$-sat $_{BIO}$ with an estimate of air–sea gas exchange rate for $O_2$ derived from a wind speed parameterization (Ho et al. 2006) from Quikscat and time-weighting technique (Reuer et al. 2007) allowed for near-continuous assessment of NCP in the surface ocean (e.g., Stanley et al. 2010, Lockwood et al. 2012). This estimate of NCP integrates over the residence time of $O_2$ in the mixed layer (8–14 d during this cruise) and is reported in mmol $O_2$ m$^{-2}$ d$^{-1}$. To convert $O_2$-based NCP to C-based NCP, we used a ratio of 1.4 $O_2$ : 1 C (Laws 1991).

We calculated a particle export (PE) ratio (Dunne et al. 2005) on the basis of the ratio of NPPp to NCP:

$$PE = NCP(mmol\ m^{-2}\ d^{-1}) / \left[ NPPp(mmol\ C\ m^{-3}\ d^{-1}) \times MLD(m) \right] \quad (3)$$

where MLD is an approximation of mixed-layer depth, leading to a simple integration of NPP to the length scale assumed by the NCP calculation. We recognize the timescale differences between EIMS-derived NCP (8–14 d) and the NPPp (1 d). Thus, our calculated PE would be analogous to export efficiency if the day's NPP was equivalent to the average NPP over the residence time of $O_2$ in the mixed layer and that the light dynamics of the MLD were sufficiently integrated over the scale of the FRRf interpolation.

MLD for the above calculation was interpolated between profiles using archived model output courtesy of the Ocean Productivity group at Oregon State University (http://www.science.oregonstate.edu/ocean.productivity/mld.html). These data are the composite of several models that define MLD on the basis of density or isotherm layer depth on the basis of temperature. We used the nearest MLD model pixel (MLD$_m$, interpolated to 18 km) and 8-d composite to the ship track and compared it with profile MLD using Levitus criteria (0.125 kg m$^{-3}$ increase from surface density). A simple quadratic function was fit, resulting in the following predictive equation: MLD$_p$ = $-6.96 + 1.69 \times$ MLD$_m$ $- 0.04 \times$ (MLD$_m$ $- 26.3)^2$; $R^2$ = 0.72, $F_{2,37}$ = 47.5, $p < 0.0001$), where MLD$_p$ is the predicted in situ MLD. Within-seascape error associated with this prediction was negligible, with the exception of

the OB seascape, where the predicted values overestimated the actual by 14% (SE = 6.8%).

*Statistics*—Mixed stepwise MLR (P$_{enter,leave}$ = 0.25) was used to determine the influence of MLDp, temperature, temperature variability, salinity, pigment diversity, diatom biomass (as proxied by [FUCO]), haptophytes biomass by [19-HEX], the percentage of Chl *a* represented by pico-, nano-, and microphytoplankton, as well as their respective Chl *a* biomasses (% $\times$ [Chl *a*]) on surface NPPp (mg C m$^{-3}$ d$^{-1}$). We then used the same MLR technique determine the influence of a subset of the above-mentioned variables and NPPp on $O_2$-sat $_{BIO}$ as a short-term indicator of NCP. The response variables were chosen on the basis of the co-occurrence of predictor variables for the surface and to minimize assumptions of mixed-layer homogeneity. Rate responses and biomass metrics were all log$_{10}$-transformed to meet assumptions of normality; a scalar of 1 was added to $O_2$-sat $_{BIO}$ to make all values > 0. For both models, regressions were conducted within each of the seascapes and across the entire study region. Predictors and thus effect sizes were normalized (centered on the mean and normalized by 0.5 of the range) to determine the relative strength of individual drivers on NPP and $O_2$-sat $_{BIO}$ and how they changed as a function of seascape. The intercept is the mean response and individual effect sizes are thus unitless and can be interpreted as the percent change in NPP or $O_2$-sat $_{BIO}$ from the mean that is associated with a percent change in the driver after accounting for weighted effects of other significant drivers.

## Results

*Seascape patterns: Physical factors, nutrients*—High-frequency surface measurements from satellite and from the ship's flow-through system revealed several meso- to gyre-scale gradients. The ship track crossed several likely eddies in the OB and SuST seascapes with anomalously high SSH (Fig. 2a) found at 30–31°N, $\sim$ 34°N, and 37°N as well as smaller anomalies associated with frontal convergences (e.g., 42°N). SSTs (Fig. 2b) were 12.8°C $\pm$ 0.8°C in the SA, rose quickly through the transition seascapes, and leveled at $\sim$ 26°C around the OB : SuST boundary (25.5°C $\pm$ 0.5°C). Sea-surface salinity (SSS, Fig. 2b; Table 3) shifts followed a similar pattern, with fresher (32.3 $\pm$ 0.1) water occurring in the SA and higher SSS (35.2 $\pm$ 0.3) in the subtropics. P$_{CO_2}$ trends have been reported elsewhere (Lockwood et al. 2012) with low concentrations with respect to the atmosphere in the SuSA seascape but the lowest concentrations occurring in the SuTR (310–
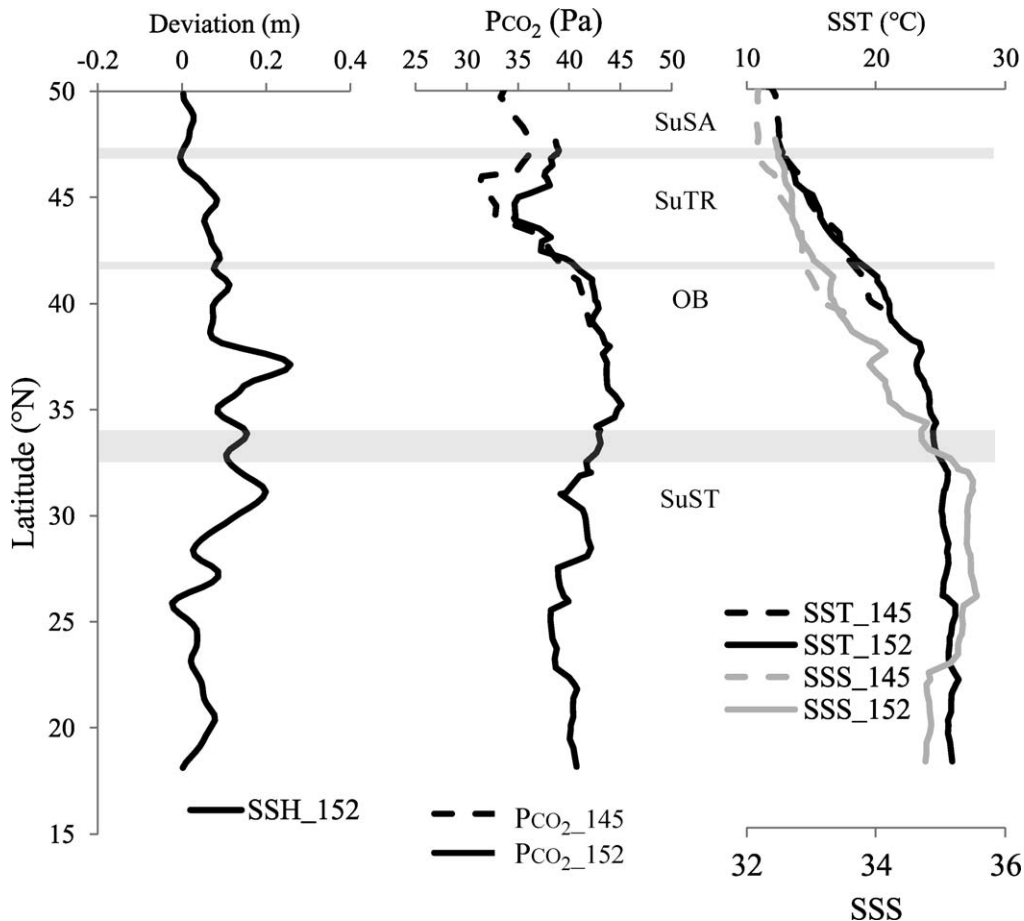
*Kavanaugh et al.*



Fig. 2.    Oceanographic and geochemical context: Latitudinal variations of SSH, SST, SSS, and $P_{CO_2}$ along 145°W and 152°W. Shaded bars denote boundaries between seascapes; bar width denotes general width of boundary. The large decrease of $P_{CO_2}$ between 42°N and 47°N is dominated by biological drawdown (Howard et al. 2010; Lockwood et al. 2012).

340 $\mu$atm; 31.4–34.5 Pa). $P_{CO_2}$ exceeded atmospheric levels south of $\sim$ 42°N, the approximate location of the SuTR : OB boundary (Fig. 2).

Macronutrient concentrations, PAR, and Chl *a* spatial patterns tended to follow the latitudinal gradients (Table 3). Nutrient concentrations were highest in the SuSA, with substantial concentrations of $NO_3$ (6.6 $\mu$mol $L^{-1}$), $PO_4$ (0.7 $\mu$mol $L^{-1}$), and $SiO_2$ (11 $\mu$mol $L^{-1}$). In the SuTR region, concentrations of major nutrients decreased to about half that of the subarctic, with the exception of $SiO_2$ (9 $\mu$mol $L^{-1}$), which was highly spatially variable. In the OB and SuST seascapes, surface nutrient concentrations were a factor of 10 less than the northern seascapes, with the exception of $SiO_2$. Mean of PAR also increased gradually from the SuSA to the SuST, with variance of PAR decreasing equatorward. Finally, Chl *a* was highest and most variable in the SuSA and decreased toward the SuST.

*Community structure and physiological status*—On basin scales, dominant phytoplankton types shifted from eukaryotic phytoplankton to prokaryotic phytoplankton at the SuTR : OB boundary (42°N), as is evident by the shifts in biomass from MV Chl *a* to DV Chl *a* (Fig. 3). In terms of size classes, nanophytoplankton were greatest contributors to eukaryotic phytoplankton biomass (as measured by percentage of total Chl *a*) across the study region (Table 3), although microphytoplankton were locally abundant in the SuTR region, with percent contribution of biomass > 30% (Table 3, Fig. 4a). Pigment diversity, as measured by the Shannon Index (Table 3), was also highest in the SuTR (2.11 $\pm$ 0.11) and almost 20% lower in the subtropics (1.75 $\pm$ 0.14).

The $\sigma_{PSII}$ generally followed the interaction of Chl *a* with PAR (Table 3, Fig. 4a), with highest values occurring in SuTR region followed by the SuSA, the OB, and then the SuST. Across the study region, Fv : Fm increased toward the subtropics, with minima of $\sim$ 0.30 during midday in the subarctic and maxima of $\sim$ 0.53 in the subtropics. (Table 3, Fig. 4b). Diurnal patterns of Fv : Fm exhibited the typical bimodal pattern of morning and evening maxima, with noontime and midnight depression of Fv : Fm (Behrenfeld et al. 2006); however, there were no distinct differences in the percent depression across seascapes (Fig. 4b).

Concentrations of both FUCO and 19-HEX were low in the SuST (Fig. 4c,d, mean ratio $\sim$ 0.3). North of $\sim$ 30°N, increases in FUCO were apparent primarily in mesoscale features that occurred at 30°N, 34°N, and 37°N where

Table 3. Summary of mean (± SE) chemical, physical, and biological properties within NE Pacific seascape surface waters. Surface properties are defined from 0 to 25 m and are a result of a combination of profile and flow-through measurements. PE ratio is derived using interpolated MLDs (*see* Methods).

| | SuSA | SuTR | OB | SuST |
|---|---|---|---|---|
| $NO_3$ ($\mu$mol L$^{-1}$) | 6.64 (2.19) | 2.45 (2.77) | 0.17 (0.27) | 0.15 (0.07) |
| $PO_4$ ($\mu$mol L$^{-1}$) | 0.72 (0.26) | 0.36 (0.30) | 0.14 (0.07) | 0.05 (0.06) |
| $NO_2^-$ ($\mu$mol L$^{-1}$) | 0.15 (0.05) | 0.05 (0.04) | 0.01 (0.02) | 0.001 (0.004) |
| $NH_4$ ($\mu$mol L$^{-1}$) | 0.14 (0.15) | 0.08 (0.08) | 0.02 (0.04) | 0.01 (0.02) |
| Silicate ($\mu$mol L$^{-1}$) | 11.17 (5.81) | 8.92 (6.03) | 3.89 (1.64) | 2.85 (1.28) |
| SST (°C) | 12.81 (0.85) | 15.34 (1.53) | 21.19 (1.91) | 25.45 (0.5) |
| Salinity | 32.30 (0.13) | 32.69 (0.16) | 33.53 (0.46) | 35.2 (0.30) |
| PAR ($\mu$E m$^{-2}$ s$^{-1}$) | 536 (161) | 656 (155) | 853 (119) | 936 (25) |
| Fv : Fm | 0.35 (0.04) | 0.36 (0.03) | 0.41 (0.03) | 0.43 (0.03) |
| $\sigma_{PSII}$ | 752 (192) | 762 (207) | 552 (95) | 502 (88) |
| $H'$ (HPLC) | 2.07 (0.13) | 2.11 (0.11) | 1.96 (0.11) | 1.75 (0.14) |
| % pico | 10.74 (19.2) | 11.8 (11.1) | 58.7 (7.9) | 66.9 (15.0) |
| % nano | 69.92 (16.6) | 57.7 (12.5) | 26.6 (10.7) | 23.1 (10.3) |
| % micro | 19.20 (6.52) | 30.32 (11.6) | 14.7 (5.9) | 9.93 (8.92) |
| Fucoxanthin ($\mu$g L$^{-1}$) | 0.13 (0.03) | 0.14 (0.02) | 0.02 (0.003) | 0.01 (0.001) |
| 19-hexanoyl fucoxanthin (g L$^{-1}$) | 0.62 (0.17) | 0.26 (0.05) | 0.03 (0.01) | 0.02 (0.003) |
| Total Chl *a*, HPLC ($\mu$g L$^{-1}$) | 0.48 (0.16) | 0.43 (0.20) | 0.09 (0.05) | 0.05 (0.01) |
| % DV Chl *a* | 0 (0) | 0.10 (1.0) | 28.8 (1.3) | 36.8 (1.0) |
| $^{14}$C (mg C m$^{-3}$ h$^{-1}$) | 2.53 (0.72) | 2.05 (1.52) | 0.80 (0.15) | 0.77 (0.09) |
| NPPp (mg C m$^{-3}$ h$^{-1}$) | 3.15 (1.60) | 3.13 (1.88) | 0.91 (0.41) | 0.53 (0.26) |
| NPPp (mg C m$^{-3}$ d$^{-1}$) | 42.5 (21.7) | 38.8 (23.4) | 11.9 (5.5) | 6.76 (3.32) |
| NPPp (mmol C m$^{-2}$ d$^{-1}$) | 74.0 (4.9) | 76.7 (7.8) | 19.6 (1.3) | 17.7 (1.5) |
| NPPp : Chl *a* (mg C mg$^{-1}$ Chl *a* d$^{-1}$) | 48 (4) | 67 (5) | 237 (15) | 334 (22) |
| Biological O$_2$ saturation (%) | 2.59 (0.83) | 2.80 (1.77) | 0.41 (0.17) | 0.55 (0.39) |
| NCP (mmol C m$^{-2}$ d$^{-1}$) | 25.1 (1.5) | 25.4 (2.0) | 6.2 (0.3) | 7.0 (0.2) |
| PE ratio | 0.25 (0.04) | 0.24 (0.02) | 0.24 (0.04) | 0.28 (0.04) |
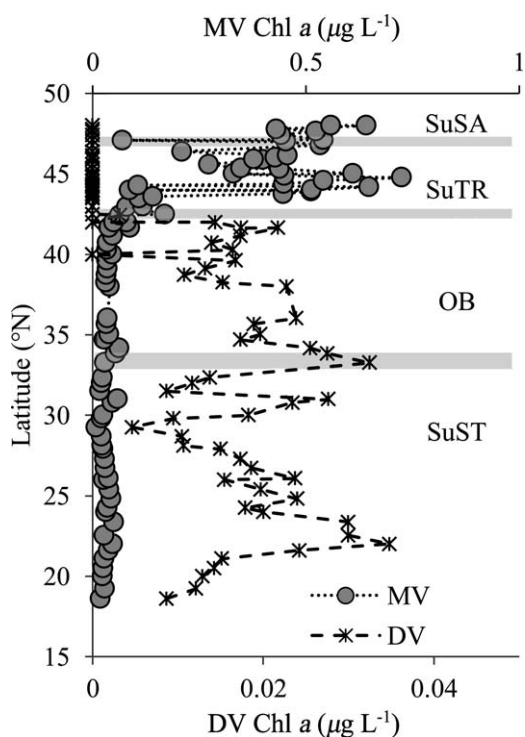


Fig. 3. Biogeographic patterns of eukaryotic (MV Chl *a*) and prochlorophyte phytoplankton (DV Chl *a*) across Northeast Pacific seascapes. Shaded bars denote boundaries between seascapes as in Fig. 1; bar width denotes qualitative width of boundary.

FUCO : 19-HEX ratios exceeded 1 : 1 (average ratio = 0.47). North of the OB : SuTR boundary, the absolute concentration of FUCO (Fig. 4b) and 19-HEX both increased, albeit the latter to a lesser degree. Thus the ratio of FUCO : 19-HEX in the SuTR (0.35) was higher than that of the SuSA (0.21).

*Primary production, community production and export efficiency*—Throughout our study region, mixed-layer NPPp and NCP were strongly coupled (Fig. 5 and Table 4: $r = 0.78$, $F_{1,146} = 230$, $p < 0.0001$); however, there was variation in the strength and sign of the correlation across seascapes. In the SuSA, the relationship tended toward neutral or negative (Table 4, $r = -0.24$ to $-0.72$); data were insufficient to determine longitudinal variability. In the SuTR, the NPPp-NCP relationship was strongly positive ($r = 0.7$, $F_{1,39} = 36.3$; $p < 0.0001$), although NCP and NPPp were more strongly coupled in the west ($r = 0.92 > r = 0.53$). Different slopes and coupling strengths between the two meridians led to a nonlinear NPPp : NCP relationship within the OB seascape. In the SuST, NPPp and NCP were strongly spatially correlated ($r = 0.68$, $F_{1,45} = 38$, $p < 0.0001$), but data were insufficient to assess east–west variability.

Rates of NPP and NCP were high in the SuSA and SuTR seascapes (Table 3, Fig. 6). Discrete measurements of NPP based on $^{14}$C incubations ranged from 2.53 mg C m$^{-3}$ in the SuSA to 0.77 mg C m$^{-3}$ in the SuST (Table 3). Interpolated NPPp revealed similar trends, albeit more
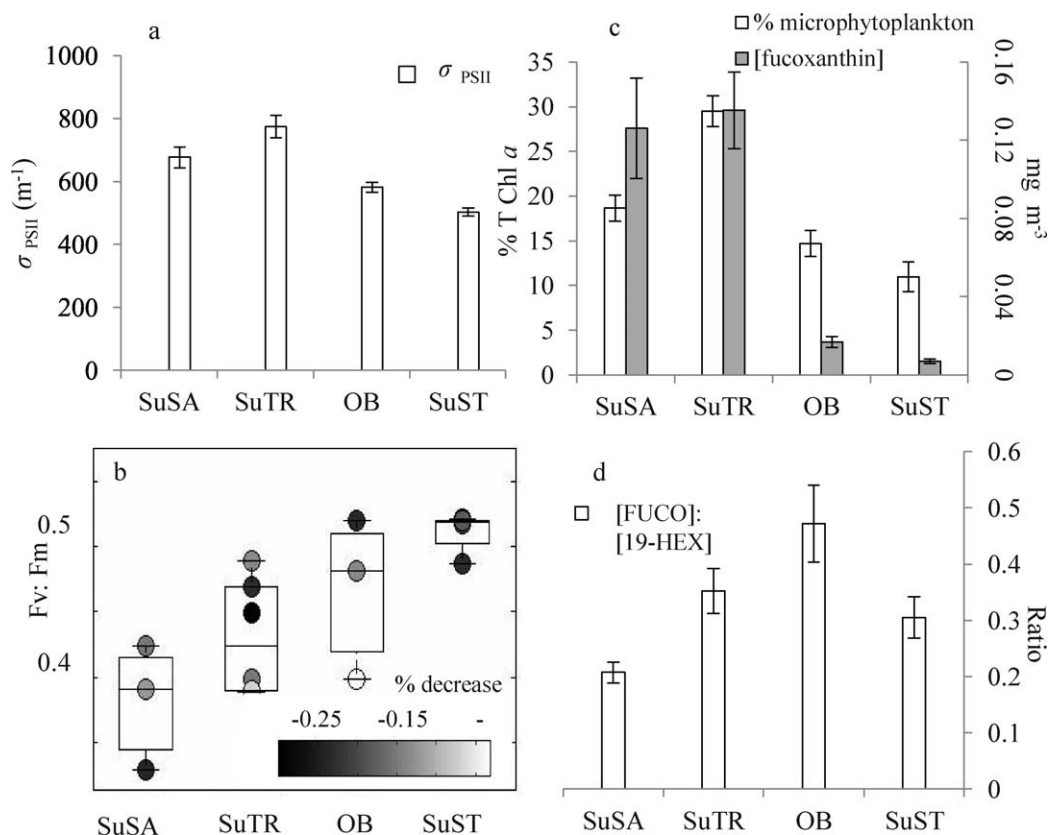
Fig. 4. Mean (± SE) biomass and physiological state of phytoplankton communities across Northeast Pacific seascapes: (a) diatom indices including percentage of total Chl *a* comprised of microphytoplankton and concentration of the indicator pigment, FUCO; (b) ratio of FUCO to 19-HEX; (c) FRRf-derived $\sigma_{PSII}$; (d) mean morning maximal Fv : Fm with color coding showing percent decrease of Fv : Fm during night.
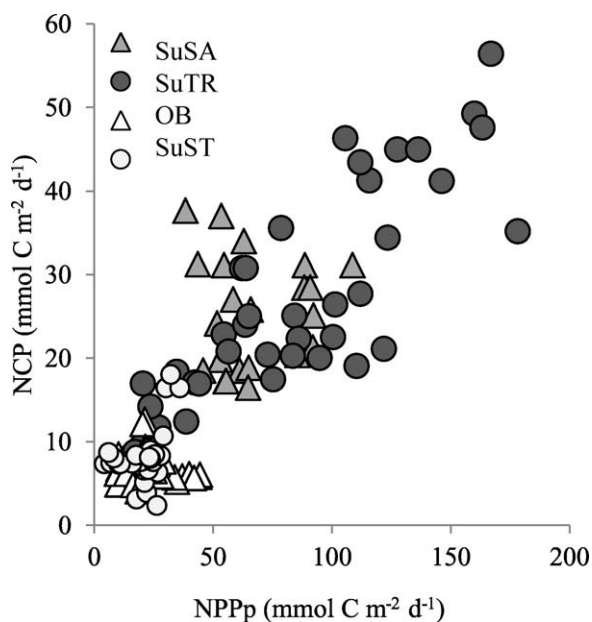


Fig. 5. Relationship between productivity measurements across Northeast Pacific seascapes. In situ net primary production (FRRf-derived proxy, NPPp) was multiplied by MLD to compare with in situ NCP as measured by $O_2$ : Ar method (*see* Methods and Lockwood et al. 2012).

variable within seascapes, with rates of exceeding 40 mg C $m^{-3}$ $d^{-1}$ in the SuSA and SuTR seascapes and decreasing to ~ 7 mg C $m^{-3}$ $d^{-1}$ in the SuST. When integrated over the mixed layer and day length (Fig. 6a), these rates were equivalent to 74 mmol C $m^{-2}$ $d^{-1}$ in the SuSA, 77 mmol C $m^{-2}$ $d^{-1}$ in the SuTR, 19 mmol C $m^{-2}$ $d^{-1}$ in the OB, and 17 mmol C $m^{-2}$ $d^{-1}$ in the SuST. Assimilation efficiency (NPPp/[Chl *a*]) was higher in the SuTR than in the SA (Table 3: 67 compared with 48 mg C [mg Chl *a*]$^{-1}$ $d^{-1}$, respectively) but was fourfold smaller than the efficiencies in the southern seascapes (Table 3: 237 and 334 mg C [mg Chl *a*]$^{-1}$ $d^{-1}$ in the OB and SuST, respectively).

NCP was generally low but positive in the SuST and OB seascapes ($O_2$-sat $_{BIO}$ = 0.55 and 0.41%, respectively; NCP = 7.7 and 6.2 mmol C $m^{-2}$ $d^{-1}$, respectively), and reached a peak between 45°N and 46°N in the SuTR seascape, although spatial variability in $O_2$-sat $_{BIO}$ and winds resulted in no differences between the geometric means of NCP in the SuTR and SuSA.

Export efficiency was relatively constant across seascapes (Table 3), although there was marked spatial variability associated with mesoscale and submesoscale features (Fig. 6b).

*Basin-wide drivers of NPP and NCP*—Across the entire study area, NPP was most strongly related to

Table 4. Spatial relationships between NPPp and NCP across and within Northeast Pacific seascapes. Correlation coefficients, $r$, slopes ($\pm$ SE), sample size ($n$), and $F$-statistics are reported for the NPPp($x$):NCP($y$) relationship across the region and for individual legs denoted by their longitude. Bolded values highlight significant correlations.

|  | $r$ | $N$ | $F$ | df | $p$ |
|---|---|---|---|---|---|
| Northeast Pacific | **0.86** | **124** | **230** | **1,122** | **<0.0001** |
| **152°W** | **0.90** | **68** | **195** | **1,66** | **<0.0001** |
| **145°W** | **0.78** | **32** | **37.6** | **1,30** | **<0.0001** |
| Subarctic (SuSA) | 0.14 | 28 | 1.8 | 1,26 | 0.19 |
| **152°W** | **0.82** | **6** | **4.34** | **1,4** | **0.05** |
| 145°W | 0.01 | 15 | 0.01 | 1,13 | 0.9 |
| Transition (SuTR) | **0.85** | **40** | **36.3** | **1,38** | **<0.0001** |
| **152°W** | **0.77** | **14** | **4.72** | **1,12** | **0.05** |
| **145°W** | **0.96** | **11** | **105** | **1,9** | **<0.0001** |
| Oligotrophic boundary (OB) | 0.15 | 33 | 0.79 | 1,31 | 0.38 |
| **152°W** | **0.44** | **20** | **4.3** | **1,18** | **0.05** |
| 145°W | 0.33 | 9 | 0.28 | 1,7 | 0.68 |
| Subtropics (SuST) | **0.58** | **46** | **13.1** | **1,44** | **<0.0001** |

microphytoplankton biomass, then nanophytoplankton biomass, a shallower MLD, and increased salinity ($R^2 = 0.90$, $p < 0.0001$, Table 5). Note that the salinity effect takes into consideration covariance with MLD across the large latitudinal extent. Increased NPP was generally associated with decreased phytoplankton diversity. O$_2$-sat $_{BIO}$ was strongly associated with NPP across the extent of our study area (Table 6). Increased O$_2$-sat $_{BIO}$ was also associated with cooler temperatures, higher salinity, increased MLD, and increased surface temperature variability. Unlike for NPP, increases in O$_2$-sat $_{BIO}$ were associated with increased phytoplankton diversity, due in part to the
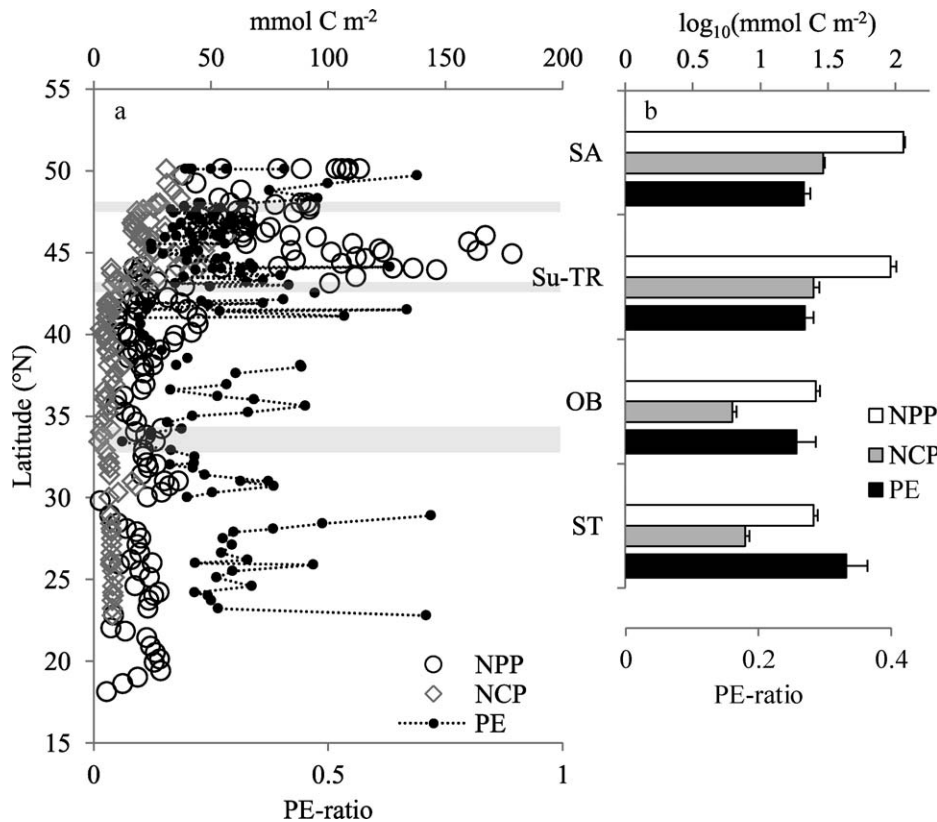


Fig. 6. NPPp, NCP, and PE efficiency across Northeast Pacific seascapes. (a) Latitudinal patterns of mixed-layer NPP, NCP, and PE; (b) mean ($\pm$ SE) mixed-layer NPPp, NCP for each seascape. Note that NPP and NCP have been log10-transformed.

Table 5. Scaled and centered effects of ecological parameters on (NPPp) within and across Northeast Pacific seascapes. Variables included in each model were determined with mixed stepwise linear regression. NPP and biomass of size classes were $\log_{10}$-transformed. All regression models are statistically significant ($p < 0.001$). Effects are significant ($p < 0.05$) unless noted with italics.

| Seascape | SuSA | SuTR | OB | SuST | Basin |
|---|---|---|---|---|---|
| $R^2$ | 0.93 | 0.92 | 0.84 | 0.61 | 0.91 |
| $R^2_{adj}$ | 0.9 | 0.91 | 0.81 | 0.58 | 0.9 |
| $N$ | 12 | 30 | 21 | 42 | 103 |
| Intercept ($\log_{10}$[mg C m$^{-3}$ d$^{-1}$]) | 1.51 (0.01) | 1.62 (0.01) | 0.91 (0.01) | 0.78 (0.03) | 1.14 (0.02) |
| MLD (m) | | | −0.16 (0.04) | −0.15 (0.04) | −0.2 (0.04) |
| SST (°C) | | 0.07 (0.03) | | | |
| SST $\sigma$ | 0.07 (0.02) | −0.10 (0.03) | | | *0.07 (0.04)* |
| Salinity | | | | | 0.18 (0.08) |
| Microphytoplankton ($\mu$g Chl $a$ L$^{-1}$) | | 0.21 (0.06) | 0.25 (0.04) | 0.31 (0.11) | 0.53 (0.08) |
| Nanophytoplankton ($\mu$g Chl $a$ L$^{-1}$) | 0.21 (0.05) | 0.31 (0.07) | | | 0.28 (0.08) |
| Picophytoplankton ($\mu$g Chl $a$ L$^{-1}$) | 0.15 (0.04) | | | 0.27 (0.11) | *0.09 (0.06)* |
| [Fucoxanthin] ($\mu$g L$^{-1}$) | | | | | |
| [19-Hexanoyl fucoxanthin] ($\mu$g L$^{-1}$) | | −0.08 (0.03) | 0.15 (0.04) | | |
| % microphytoplankton | | | −0.10 (0.04) | | |
| % nanophytoplankton | | | | | |
| % picophytoplankton | | | | | |
| $H'$ HPLC | | | | −0.21 (0.08) | −0.19 (0.05) |

large spatial extent but also potentially the time lag associated with the particular measurement of NCP.

*Seascape drivers of NPP and NCP*—The source of variation and forcing strength of both NPP and O$_2$-sat $_{BIO}$ were different across seascapes, reflecting variability in physical and ecological drivers within water masses.

In the SuSA seascape, NPP was associated with increased nano- and picophytoplankton biomass and decreased temperature variability (Table 5). Increased O$_2$-sat $_{BIO}$ in the SuSA (Table 6) was associated with cooler temperatures, decreased salinity, and decreased NPP, with the latter likely indicative of bloom decay. Although decreased MLD was included as part of the stepwise procedure, MLD was not a significant driver of NPP or NCP in the subarctic.

NPP in the SuTR was driven primarily by increases in nano- and microphytoplankton biomass (Table 5), although the biomass of specific nanophytoplankton (e.g., coccolithophores) with high concentrations of 19-HEX was negatively correlated with NPP. NPP was also associated with local increases in SST and decreases in temperature variability. Increased NCP within the SuTR was strongly associated with fresher water (Table 5) and warmer temperatures. Increased NCP was also driven by increased NPP and increases in FUCO, the biomarker specific to diatoms in this region.

In the OB, increased NPP was associated with increased microphytoplankton biomass and shallower mixed layers. However, the taxon effect was complex, with NPP driven also by decreases in the biomarker 19-HEX and percent contribution or dominance by microphytoplankton. NCP

Table 6. Scaled and centered effects of ecological parameters on net community production (NCP) within and across Northeast Pacific seascapes. Variables included in each model were determined with mixed stepwise linear regression. NCP was measured by O$_2$-sat $_{BIO}$. NCP, NPP, and biomass of size classes were $\log_{10}$-transformed. Effects are significant ($p < 0.05$) unless noted with italics.

| Seascape | SuSA | SuTR | OB | SuST | Basin |
|---|---|---|---|---|---|
| $R^2$ | 0.87 | 0.71 | 0.76 | 0.81 | 0.79 |
| $R^2_{adj}$ | 0.85 | 0.64 | 0.72 | 0.78 | 0.78 |
| $N$ | 12 | 30 | 21 | 42 | 103 |
| Intercept ($\log_{10}$[% saturation + 1]) | 0.54 (0.01) | 0.58 (0.02) | 0.16 (0.04) | 0.18 (0.01) | 0.33 (0.01) |
| NPP ($\log_{10}$[mg C m$^{-3}$ d$^{-1}$]) | −0.09 (0.02) | 0.13 (0.06) | 0.11 (0.03) | *0.04 (0.02)* | 0.26 (0.06) |
| MLD (m) | *−0.02 (0.02)* | *−0.02 (0.07)* | | −0.05 (0.02) | 0.09 (0.02) |
| SST (°C) | 0.11 (0.03) | 0.34 (0.09) | −0.06 (0.02) | 0.09 (0.02) | −0.17 (0.05) |
| SST $\sigma$ | | | 0.05 (0.01) | 0.03 (0.01) | |
| Salinity | −0.06 (0.03) | 0.56 (0.15) | | 0.04 (0.01) | 0.20 (0.05) |
| Microphytoplankton ($\mu$g Chl $a$ L$^{-1}$) | | | | 0.08 (0.02) | 0.12 (0.05) |
| Nanophytoplankton ($\mu$g Chl $a$ L$^{-1}$) | | | −0.07 (0.04) | *0.05 (0.03)* | |
| Picophytoplankton ($\mu$g Chl $a$ L$^{-1}$) | | | | 0.10 (0.02) | |
| [Fucoxanthin] ($\mu$g L$^{-1}$) | | 0.15 (0.06) | | | |
| [19-Hexanoyl fucoxanthin] ($\mu$g L$^{-1}$) | | | | | |
| % microphytoplankton | | | | | |
| % nanophytoplankton | | | | | |
| % picophytoplankton | | *0.10 (0.06)* | | | |
| $H'$ HPLC | | | | | 0.10 (0.03) |

in the OB was driven almost equally by NPP and increases in phytoplankton diversity.

In the SuST, increased NPP was associated with increased microphytoplankton or picophytoplankton biomass and shallower mixed layers. The negative effect of phytoplankton diversity suggested that increased NPP was likely associated with blooms of either microphytoplankton or picophytoplankton, not both. The drivers of NCP in the SuST were complex, with positive effects associated with warmer and less variable temperatures, increased salinity, and to a lesser degree, shallower MLDs. Increased NCP was also supported somewhat by increases in picophytoplankton, microphytoplankton, and nanophytoplankton biomass, although the latter was not significant.

## Discussion

In this study, we utilized an objective seascape framework to evaluate the spatial variability and role of different drivers of NPP and NCP across the Northeast Pacific. We evaluated these drivers in a systematic and quantitative fashion to lend inference to future modeling efforts and field campaigns. Although this cruise represents a snapshot in time, the results taken in the context of the large spatial extent as well as additional modeling efforts (Lockwood et al. 2012) provide insight into the functioning of this geochemically and ecologically important region. Specifically, it focuses our attention on emergent properties of the transition zone where the magnitude, efficiency, and taxonomic composition of the biological pump may act in synergy to affect air–sea $CO_2$ exchange.

*Biogeochemical rates*—Both NPP and NCP were high across the SuSA and SuTR seascapes. Mean NPP in the SA was > 25% higher than previously measured for a similar time of year (30 mg m$^{-3}$ d$^{-1}$; Boyd and Harrison 1999), with some areas exhibiting twofold higher NPP. In contrast, our NPP estimates in the OB and SuST seascapes outside the eddies were similar to the rates reported at Sta. ALOHA (22°45′N, 158°W) as measured by 12 h $^{14}$C incubations (average 7 mg C m$^{-3}$ d$^{-1}$ in August and 6 mg C m$^{-3}$ d$^{-1}$ in September). Average seascape PE was relatively high (> 0.2) but consistent with other measurements using $O_2$:Ar-based NCP (Stanley et al. 2010; Huang et al. 2012).

Regression model results suggest that a seascape approach may improve parameterization of predictive models in the region. However, three uncertainties remain: (1) mesoscale perturbations, not resolved in the current classification, may locally affect both nutrient requirements and export efficiency; (2) subsurface dynamics of particle export, particularly below the seasonal mixed layer, are not well resolved in the measurements (Buessler and Boyd 2009; Howard et al. 2010); and (3) spatial relationships may reflect differences in the timescales for the measurements of NPP and NCP. Specifically, rates of NCP in the SuSA may have been affected by the Kasatochi volcano eruption 3 weeks prior (Hamme et al. 2010). Because of the longer integration time of $O_2$, NCP could reflect this high-productivity event, whereas the signature would not be evident in the NPPp measurements. In the SuTR, high NPP and NCP are likely persistent characteristics of that seascape, particularly through spring and summer, as it is supported from cruise- and satellite-based studies (Juranek et al. 2012; Kavanaugh et al. 2014) and model results (Lockwood et al. 2012). Along with depth-integrated observations, these uncertainties can be addressed in the future by coupling feature tracking (e.g., eddies; Gaube et al. 2013) and physiological metrics from space (Behrenfeld et al. 2009) across the broad ecosystem variation that seascapes represent.

*Physicochemical drivers*—Hydrography and biogeochemistry may play a role in the persistently high NPP and NCP found in the SuTR. On regional scales, the northern SuSA seascape has long been known to exhibit iron limitation, leading to excess surface macronutrients (e.g., Boyd et al. 2004). Besides via volcanic eruption (Hamme et al. 2010; Langmann et al. 2010), episodic delivery of iron to the SuSA and SuST can occur via atmospheric deposition (Mahowald et al. 2009; Crusius et al. 2011), advection from the continental shelf (Crawford et al. 2002; Lam et al. 2006) resulting in meso- to local-scale input of new micronutrients. Southward Ekman transport of subarctic water mixing with relatively iron-replete subtropical water has also been suggested to drive the location of the TZCF (Ayers and Lozier 2010), a cross-basin feature defined by a sharp gradient in Chl *a* (Polovina et al. 2001) and approximated by the SuST and OB boundary (Kavanaugh et al. 2014). Peaks in macronutrient transport occur in the eastern subarctic boundary region in late summer (Ayers and Lozier 2010), coincident with the timing of our cruise. Lockwood et al. (2012) also hypothesized that frontogenesis near 152°W in the SuTR could contribute to a persistent new nutrient supply. Because of the timescale of NCP measurements, we cannot disentangle in our analysis whether the strong association of NCP with fresher water is a result of southward mixing of fresher subarctic water or a result of a spatiotemporal lag following divergence. Certainly the high rates of NPPp along 152°W would support the latter, as that measurement is not subject to the longer timescales. Likely, several hydrographical factors at multiple scales may interact within the SuTR, contributing to biogeochemical optimum in which nitrate-replete subarctic waters encounter sufficient iron to support high rates of NPP, moderate efficiency through diatom sinking, and subsequent high rates of NCP.

MLD has long been considered an important driver of regional and global NPP and NCP (e.g., Sverdrup 1953; Polovina et al. 1995). Within the subarctic Pacific, summer warming and subsequent shoaling of the mixed layer peaks in August (e.g., Whitney 2011). The mixed layer in this region can shoal in association with freshwater influx from the continental shelf (Whitney 2011); in this case both light and micronutrient availability for phytoplankton increases. In the subtropics, mixed-layer and nutrient dynamics within mesoscale eddies have long been hypothesized to play a role in productivity and export (Letelier et al. 2000; Johnson et al. 2010). In our study, MLD was important in driving NPP and NCP on basin scales but the within-seascape results were variable, with MLD revealed as an

important driver in the OB and SuST seascapes. This may be due to the fact that subtropical mesoscale features have a distinct spatial signature, whereas the longer-term spatially coherent processes in the northern seascapes would be less apparent during the snapshot of our cruise.

*Macrophysiological patterns*—Global-scale physiological analyses depict the North Pacific transition as a region that is relatively replete in both macronutrients and micronutrients (Behrenfeld et al. 2009). In our study, variable fluorescent patterns were different across seascapes, indicative of regional variability in chronic nutrient limitation (Suzuki et al. 2002; Behrenfeld et al. 2006). The SuTR seascape had intermediate Fv : Fm relative to the low SuSA and higher OB and SuST seascapes, on average, and particularly when considering only local morning maxima. In general, assimilation efficiencies (NPP : Chl *a*) were higher in the SuTR than in the SuSA, suggesting higher growth rates in the SuTR relative to the SuSA. On diurnal scales large nighttime depression in Fv : Fm can be attributed to depletion of the plastiquinone pools through iron stress and high growth rates (Behrenfeld et al. 2006; Behrenfeld and Milligan 2013). However, there were no coherent biogeographical patterns of iron stress across seascapes in our study region, contrary to other studies in the subtropical and equatorial Pacific (Strutton et al. 2004; Behrenfeld et al. 2006). Finally, where the larger size structure and increased PAR in the SuTR might predict decreased $\sigma_{PSII}$, $\sigma_{PSII}$ increased, suggesting an increase in the number or functioning of light-harvesting complexes. These observations coupled with near-Redfield drawdown of nitrate in the SuTR support the notion that the SuTR envelopes a biogeochemical optima where high growth rates are supported by sufficient, albeit patchy, supplies of new nutrients.

*Ecological drivers*—Researchers have focused on shifts in export production driven by temperature (Laws et al. 2000), food-web structure (Legendre 2002; Dunne et al. 2005), and new nutrients (Karl et al. 2012). Several characteristics contribute to PE efficiency, including ballasting, fecal packaging, and episodic events that decouple autotrophic and heterotrophic processes. In our study, spatial patterns across and within seascapes indicate the relative importance of the different physiological and ecological drivers that contribute to NPP and NCP. More important, drivers are scale dependent and vary from the basin to the seascape. In the SuTR seascape, warmer temperatures, high nanophytoplankton biomass, and high microphytoplankton biomass led to high NPP, and in turn, high NPP, warmer temperatures, higher salinity, and specifically diatoms contributed to high NCP.

The effect of phytoplankton community structure on export production is complex and can affect both the input by NPP as well as the efficiency of the biological pump. Taxa with mineral ballasting, e.g., diatoms and coccolithophores, may contribute disproportionately to export (Armstrong et al. 2001). It has also been suggested that all phytoplankton contribute to export production proportionally to their primary production (Richardson and Jackson 2007), with increased export associated with aggregation or packaging in fecal matter. Diversity can also play a role in carbon production and export by maximizing nutrient use efficiency (Ptacnik et al. 2008) and by affecting the spatial and temporal coupling between autotrophic and heterotrophic processes. After accounting for the effects of hydrography, size structure, and specific ballasting taxa, we found that phytoplankton pigment diversity was negatively correlated with NPPp at basin scales (i.e., across all seascapes) and within-seascape production was driven by a few dominant groups. Diversity was not a significant driver of NCP within any seascape but was positively correlated with NCP at basin scales. Like NCP, diversity peaked in the transition zone; however, taxonomic drivers of NCP were limited to diatoms in this geochemically important seascape.

*The biological pump in the transition seascape*—The magnitude of NPP, moderate export efficiency, and phytoplankton community composition contribute in synergy to the SuTR role as a sink for atmospheric $CO_2$. High NPP in the SuTR was associated with high NCP, leaving little assimilated carbon to be respired in the surface. Although within-seascape NPP was driven by nano- and microphytoplankton, only diatoms were taxon-specific drivers of NCP. Sediment trap data suggest $CaCO_3$ to be a more efficient ballast mineral than $SiO_2$ (Brix et al. 2006), leading to greater POC export associated with coccolithophores; however, the loss of alkalinity can result in decreased pH and increased $P_{CO_2}$ in surface waters, thus negating the biological pump's effect on DIC drawdown. Pigment analysis suggested that the diatom-to-coccolithophore ratio, although highest in the OB, was moderately high in the SuTR. Thus if this pattern persisted over month scales, the air–sea exchange associated with biological drawdown of DIC by diatoms would not be affected by losses in alkalinity (and increases in surface $P_{CO_2}$), as would occur with coccolithophore-based production.

Given potential shifts in ecosystem functioning associated with ocean acidification, temperature, or expansion of oligotrophic boundaries, understanding how water masses respond and modulate perturbations at different scales becomes increasingly important. The recurrence of high NPP, the strong coupling between NPP and NCP, the diatom-based export, and the importance of biologically mediated air–sea exchange of $CO_2$ (Howard et al. 2010; Lockwood et al. 2012) suggest that the North Pacific transition seascape is a region where biochemical and ecological interactions in the surface plankton community are profoundly important for modulating the carbon pump. Decreases in NPP in the transition are projected with global warming (Polovina et al. 2011). However, the location and extent of the transition zone may be affected by climate oscillations (Chai et al. 2003; Di Lorenzo et al. 2008) or by temperature-related expansion of the subtropics (Polovina et al. 2008; Irwin and Oliver 2009). Future scenarios also do not account for changes in iron deposition associated with shifts in the westerlies (Mahowald et al. 2009), leading to much uncertainty in predicting future shifts in the functioning of the biological pump and

its role in air–sea exchange. Thus, although more research is needed in this ecologically and geochemically important zone, we assert that the systematic seascape approach that we have used and our subsequent results will inform future modeling and ship-based efforts that will illuminate the spatiotemporal variability of the functioning of the biological pump on interannual to climate scales.

# References

ARMSTRONG, R. A., C. LEE, J. I. HEDGES, S. HONJO, AND S. G. WAKEHAM. 2001. A new, mechanistic model for organic carbon fluxes in the ocean based on the quantitative association of POC with ballast minerals. Deep Sea Res. II **49:** 219–236, doi:10.1016/S0967-0645(01)00101-1

AYERS, J. M., AND M. S. LOZIER. 2010. Physical controls on the seasonal migration of the North Pacific transition zone chlorophyll front. J. Geophys. Res. **115:** C05001, doi:10.1029/2009JC005596

BEHRENFELD, M. J., AND A. J. MILLIGAN. 2013. Photophysiological expressions of iron stress in phytoplankton. Annu. Rev. Mar. Sci. **5:** 217–246, doi:10.1146/annurev-marine-121211-172356

———, K. WORTHINGTON, R. M. SHERRELL, F. P. CHAVEZ, P. STRUTTON, M. McPHADEN, AND D. M. SHEA. 2006. Controls on tropical Pacific Ocean productivity revealed through nutrient stress diagnostics. Nature **442:** 1025–1028, doi:10.1038/nature05083

———, AND OTHERS. 2009. Satellite-detected fluorescence reveals global physiology of ocean phytoplankton, Biogeosciences **6:** 779–794, doi:10.5194/bg-6-779-2009

BOYD, P. W., AND P. J. HARRISON. 1999. Phytoplankton dynamics in the NE subarctic Pacific. Deep Sea Res. II **46:** 2405–2432, doi:10.1016/S0967-0645(99)00069-7

———, AND OTHERS. 2004. The decline and fate of an iron-induced subarctic phytoplankton bloom. Nature **428:** 549–53, doi:10.1038/nature02437

BRICAUD, A., H. CLAUSTRE, J. RAS, AND K. OUBELKHEIR. 2004. Natural variability of phytoplanktonic absorption in oceanic waters: Influence of the size structure of algal populations. J. Geophys. Res. **109:** C11010, doi:10.1029/2004JC002419

BRIX, H., N. GRUBER, D. M. KARL, AND N. R. BATES. 2006. On the relationships between primary, net community, and export production in subtropical gyres. Deep Sea Res. II **53:** 698–717, doi:10.1016/j.dsr2.2006.01.024

BUESSELER, K. O., AND P. W. BOYD. 2009. Shedding light on processes that control particle export and flux attenuation in the twilight zone of the open ocean. Limnol. Oceanogr. **54:** 1210–1232, doi:10.4319/lo.2009.54.4.1210

CASSAR, N., B. A. BARNETT, M. L. BENDER, J. KAISER, R. C. HAMME, AND B. TILBROOK. 2009. Continuous high-frequency dissolved O$_2$/Ar measurements by equilibrator inlet mass spectrometry. Anal. Chem. **81:** 1855–1864, doi:10.1021/ac802300u

CHAI, F., M. JIANG, R. BARBER, R. DUGDALE, AND Y. CHAO. 2003. Interdecadal variation of the transition zone chlorophyll front: A physical–biological model simulation between 1960 and 1990. J. Oceanogr. **59:** 461–475, doi:10.1023/A:1025540632491

CORNO, G., R. M. LETELIER, M. R. ABBOTT, AND D. M. KARL. 2006. Assessing primary production variability in the North Pacific Subtropical Gyre: A comparison of fast repetition rate fluorometry and $^{14}$C measurements. J. Phycol. **42:** 51–60, doi:10.1111/j.1529-8817.2006.00163.x

CRAWFORD, W. R. 2002. Physical characteristics of Haida eddies. J. Oceanography **58:** 703–713, doi:10.1023/A:1022898424333

CRUSIUS, J., A. W. SCHROTH, S. GASS, C. M. MOY, R. C. LEVY, AND M. GATICA. 2011. Glacial flour dust storms in the Gulf of Alaska: Hydrologic and meteorological controls and their importance as a source of bioavailable iron. Geophys. Res. Lett. **38:** L06602, doi:10.1029/2010GL046573

DANDONNEAU, Y., Y. MONTEL, J. BLANCHOT, J. GIRAUDEAU, AND J. NEVEUX. 2006. Temporal variability in phytoplankton pigments, picoplankton and coccolithophores along a transect through the North Atlantic and tropical southwestern Pacific. Deep Sea Res. I **53:** 689–712, doi:10.1016/j.dsr.2006.01.002

DE LA ROCHA, C. L., AND U. PASSOW. 2007. Factors influencing the sinking of POC and the efficiency of the biological carbon pump. Deep Sea Res. II **54:** 639–658, doi:10.1016/j.dsr2.2007.01.004

DI LORENZO, E., AND OTHERS. 2008. North Pacific Gyre Oscillation links ocean climate and ecosystem change. Geophys. Res. Lett. **35:** L08607, doi:10.1029/2007GL032838

DUARTE, C. M., AND A. REGAUDIE DE GIOUX. 2009. Thresholds of gross primary production for the metabolic balance of marine planktonic communities. Limnol. Oceanogr. **54:** 1015–1022, doi:10.4319/lo.2009.54.3.1015

DUNNE, J. P., R. A. ARMSTRONG, A. GNANADESIKAN, AND J. L. SARMIENTO. 2005. Empirical and mechanistic models for the particle export ratio. Global Biogeochem. Cycles **19:** GB4026, doi:10.1029/2004GB002390

EMERSON, S., P. QUAY, D. KARL, C. WINN, L. TUPAS, AND M. LANDRY. 1997. Experimental determination of the organic carbon flux from open-ocean surface waters. Nature **389:** 951–954, doi:10.1038/40111

FALKOWSKI, P. G., R. T. BARBER, AND V. SMETACEK. 1998. Biogeochemical controls and feedbacks on ocean primary production. Science **281:** 200–206, doi:10.1126/science.281.5374.200

FEELY, R. A., R. WANNINKHOF, H. B. MILBURN, C. E. COSCA, M. STAPP, AND P. MURPHY. 1998. A new automated underway system for making high-precision P$_{CO_2}$ measurements onboard research ships. Anal. Chim. Acta **377:** 185–191, doi:10.1016/S0003-2670(98)00388-2

GAUBE, P., D. B. CHELTON, P. G. STRUTTON, AND M. J. BEHRENFELD. 2013. Satellite observations of chlorophyll, phytoplankton biomass, and Ekman pumping in nonlinear mesoscale eddies. J. Geophys. Res. **118:** 6349–6370, doi:10.1002/2013JC009027

GOERICKE, R., AND D. J. REPETA. 1992. The pigments of *Prochlorococcus marinus*: The presence of divinyl chlorophyll *a* and *b* in a marine procaryote. Limnol. Oceanogr. **37:** 425–433, doi:10.4319/lo.1992.37.2.0425

HALSEY, K. H., A. J. MILLIGAN, AND M. J. BEHRENFELD. 2010. Physiological optimization underlies growth rate-independent chlorophyll-specific gross and net primary production. Photosynth. Res. **103:** 125–137, doi:10.1007/s11120-009-9526-z

HAMA, T., T. MIYAZAKI, Y. OGAWA, T. IWAKUMA, M. TAKAHASHI, A. OTSUKI, AND S. ICHIMURA. 1983. Measurement of photosynthetic production of a marine phytoplankton population using a stable $^{13}C$ isotope. Mar. Biol. **73**: 31–36, doi:10.1007/BF00396282

HAMME, R. C., AND OTHERS. 2010. Volcanic ash fuels anomalous plankton bloom in subarctic northeast Pacific. Geophys. Res. Lett. **37**: L19604, doi:10.1029/2010GL044629

HO, D. T., C. S. LAW, M. J. SMITH, P. SCHLOSSER, M. HARVEY, AND P. HILL. 2006. Measurements of air-sea gas exchange at high wind speeds in the Southern Ocean: Implications for global parameterizations. Geophy. Res. Lett. **33**: L16611, doi:10.1029/2006GL026817

HOWARD, E., S. EMERSON, S. BUSHINSKEY, AND C. STUMP. 2010. The role of net community production in air–sea carbon fluxes at the North Pacific subarctic–subtropical boundary region. Limnol. Oceanogr. **55**: 2585–2596, doi:10.4319/lo.2010.55.6.2585

HUANG, K., H. DUCKLOW, M. VERNET, N. CASSAR, AND M. L. BENDER. 2012. Export production and its regulating factors in the West Antarctica Peninsula region of the Southern Ocean. Global Biogeochem. Cycles **26**: GB2005, doi:10.1029/2010GB004028

IRWIN, A. J., AND M. J. OLIVER. 2009. Are ocean deserts getting larger? Geophys. Res. Lett. **36**: L18609, doi:10.1029/2009GL039883

JASSBY, A. D., AND T. PLATT. 1976. Mathematical formulation of the relationship between photosynthesis and light for phytoplankton. Limnol. Oceanogr. **21**: 540–547, doi:10.4319/lo.1976.21.4.0540

JOHNSON, K. S., S. C. RISER, AND D. M. KARL. 2010. Nitrate supply from deep to near-surface waters of the North Pacific subtropical gyre. Nature **465**: 1062–1065, doi:10.1038/nature09170

JURANEK, L. W., P. D. QUAY, R. A. FEELY, D. LOCKWOOD, D. M. KARL, AND M. J. CHURCH. 2012. Biological production in the NE Pacific and its influence on air–sea $CO_2$ flux: Evidence from dissolved oxygen isotopes and $O_2/Ar$. J. Geophys. Res. **117**: C05022.

KARL, D. M., M. J. CHURCH, J. E. DORE, R. M. LETELIER, AND C. MAHAFFEY. 2012. Predictable and efficient carbon sequestration in the North Pacific Ocean supported by symbiotic nitrogen fixation. Proc. Nat. Acad. Sci. USA **109**: 1842–1849, doi:10.1073/pnas.1120312109

KAVANAUGH, M. T., B. HALES, M. SARACENO, Y. H. SPITZ, A. E. WHITE, AND R. M. LETELIER. 2014. Hierarchical and dynamic seascapes: A quantitative framework for scaling pelagic biogeochemistry and ecology. Prog. Oceanogr. **120**: 291–304, doi:10.1016/j.pocean.2013.10.013

KOLBER, Z. S., O. PRÁŠIL, AND P. G. FALKOWSKI. 1998. Measurements of variable chlorophyll fluorescence using fast repetition rate techniques: Defining methodology and experimental protocols. Biochim. Biophys. Acta **1367**: 88–106, doi:10.1016/S0005-2728(98)00135-2

LAM, P. J., J. K. BISHOP, C. C. HENNING, M. A. MARCUS, G. A. WAYCHUNAS, AND I. Y. FUNG. 2006. Wintertime phytoplankton bloom in the subarctic Pacific supported by continental margin iron. Glob. Biogeochem. Cy. **20**: GB1006, doi:10.1029/2005GB002557

LANGMANN, B., K. ZAKŠEK, M. HORT, AND S. DUGGEN. 2010. Volcanic ash as fertiliser for the surface ocean. Atm. Chem. Phys. **10**: 3891–3899.

LAWS, E. A. 1991. Photosynthetic quotients, new production and net community production in the open ocean. Deep Sea Res. I **38**: 143–167, doi:10.1016/0198-0149(91)90059-O

———, P. G. FALKOWSKI, W. O. SMITH, JR., H. DUCKLOW, AND J. J. MCCARTHY. 2000. Temperature effects on export production in the open ocean. Global Biogeochem. Cycles **14**: 1231–1246, doi:10.1029/1999GB001229

LEGENDRE, L. 2002. Fluxes of carbon in the upper ocean: Regulation by food-web control nodes. Mar. Ecol. Prog. Ser. **242**: 95–109, doi:10.3354/meps242095

LETELIER, R. M., D. M. KARL, M. R. ABBOTT, P. FLAMENT, M. FREILICH, R. LUKAS, AND T. STRUB. 2000. Role of late winter mesoscale events in the biogeochemical variability of the upper water column of the North Pacific Subtropical Gyre. J. Geophys. Res.: Oceans **105**: 28,723–28,739, doi:10.1029/1999JC000306

LOCKWOOD, D., P. D. QUAY, M. T. KAVANAUGH, L. W. JURANEK, AND R. FEELY. 2012. Influence of net community production on air–sea $CO_2$ flux in the Northeast Pacific. Global Biogeochem. Cycles **26**: GB4010, doi:10.1029/2012GB004380

LOPEZ-URRUTIA, A., E. SAN MARTIN, R. P. HARRIS, AND X. IRIGOIEN. 2006. Scaling the metabolic balance of the oceans. Proc. Natl. Acad. Sci. USA **103**: 8739–8744, doi:10.1073/pnas.0601137103

MAHOWALD, N. M., AND OTHERS. 2009. Atmospheric iron deposition: Global distribution, variability, and human perturbations. Annu. Rev. Mar. Sci. **1**: 245–278, doi:10.1146/annurev.marine.010908.163727

MALDONADO, M. T., P. W. BOYD, P. J. HARRISON, AND N. M. PRICE. 1999. Co-limitation of phytoplankton growth by light and Fe during winter in the NE subarctic Pacific Ocean. Deep Sea Res. II **46**: 2475–2485, doi:10.1016/S0967-0645(99)00072-7

MARGALEF, R. 1968. Perspectives in ecological theory. Univ. of Chicago Press.

MARRA, J. 2009. Net and gross productivity: Weighing in with $^{14}C$. Aquat. Microb. Ecol. **56**: 123–131, doi:10.3354/ame01306

MONAHAN, A. H., AND K. L. DENMAN. 2004. Impacts of atmospheric variability on a coupled upper-ocean/ecosystem model of the subarctic Northeast Pacific. Global Biogeochem. Cycles **18**: GB2010, doi:10.1029/2003GB002100

POLOVINA, J. J., J. P. DUNNE, P. A. WOODWORTH, AND E. A. HOWELL. 2011. Projected expansion of the subtropical biome and contraction of the temperate and equatorial upwelling biomes in the North Pacific under global warming. ICES J. Mar. Sci. J. Conseil **68**: 986–995, doi:10.1093/icesjms/fsq198

———, E. A. HOWELL, AND M. ABECASSIS. 2008. Ocean's least productive waters are expanding. Geophys. Res. Lett. **35**: L03618, doi:10.1029/2007GL031745

———, ———, D. R. KOBAYASHI, AND M. P. SEKI. 2001. The transition zone chlorophyll front, a dynamic global feature defining migration and forage habitat for marine resources. Prog. Oceanogr. **49**: 469–483, doi:10.1016/S0079-6611(01)00036-2

———, G. T. MITCHUM, AND G. T. EVANS. 1995. Decadal and basin-scale variation in mixed layer depth and the impact on biological production in the Central and North Pacific, 1960–88. Deep Sea Res. I **42**: 1701–1716, doi:10.1016/0967-0637(95)00075-H

PTACNIK, R., AND OTHERS. 2008. Diversity predicts stability and resource use efficiency in natural phytoplankton communities. Proc. Natl. Acad. Sci. USA **105**: 5134–5138, doi:10.1073/pnas.0708328105

REUER, M. K., B. A. BARNETT, M. L. BENDER, P. G. FALKOWSKI, AND M. B. HENDRICKS. 2007. New estimates of Southern Ocean biological production rates from $O_2/Ar$ ratios and the triple isotope composition of $O_2$. Deep Sea Res. I **54**: 951–974, doi:10.1016/j.dsr.2007.02.007

RICHARDSON, T. L., AND G. A. JACKSON. 2007. Small phytoplankton and carbon export from the surface ocean. Science **315**: 838–840, doi:10.1126/science.1133471

SERRET, P., E. FERNANDEZ, AND C. ROBINSON. 2002. Biogeographic differences in the net metabolism of the open ocean. Ecology **83:** 3225–3234, doi:10.1890/0012-9658(2002)083[3225:BDITNE]2.0.CO;2

SIEGENTHALER, U., AND J. L. SARMIENTO. 1993. Atmospheric carbon dioxide and the ocean. Nature **365:** 119–125, doi:10.1038/365119a0

STANLEY, R. H. R., J. B. KIRKPATRICK, N. CASSAR, B. A. BARNETT, AND M. B. BENDER. 2010. Net community production and gross primary production rates in the western equatorial Pacific. Global Biogeochem. Cycles **24:** GB4001, doi:10.1029/2009GB003651

STRUTTON, P. G., F. P. CHAVEZ, R. C. DUGDALE, AND V. HOGUE. 2004. Primary productivity in the central equatorial Pacific (3°S, 130°W) during GasEx-2001. J. Geophys. Res. **109:** C08S06, doi:10.1029/2003JC001790

SUGGETT, D. J., C. M. MOORE, A. E. HICKMAN, AND R. J. GEIDER. 2009. Interpretation of fast repetition rate (FRR) fluorescence: Signatures of phytoplankton community structure versus physiological state. Mar. Ecol. Prog. Ser. **376:** 1–19, doi:10.3354/meps07830

SUZUKI, K., AND OTHERS. 2002. East–west gradients in the photosynthetic potential of phytoplankton and iron concentration in the subarctic Pacific Ocean during early summer. Limnol. Oceanogr. **47:** 1581–1594, doi:10.4319/lo.2002.47.6.1581

SVERDRUP, H. U. 1953. On conditions for the vernal blooming of phytoplankton. J. Conseil **18:** 287–295, doi:10.1093/icesjms/18.3.287

TAKAHASHI, T., AND OTHERS. 2002. Global sea–air CO$_2$ flux based on climatological surface ocean pCO$_2$, and seasonal biological and temperature effects. Deep Sea Res. II **49:** 1601–1622, doi:10.1016/S0967-0645(02)00003-6

———, AND ———. 2009. Climatological mean and decadal change in surface ocean pCO$_2$, and net sea–air CO$_2$ flux over the global oceans. Deep Sea Res. II **56:** 554–577, doi:10.1016/j.dsr2.2008.12.009

UITZ, J., H. CLAUSTRE, A. MOREL, AND S. HOOKER. 2006. Vertical distribution of phytoplankton communities in open ocean: An assessment based on surface chlorophyll. J. Geophys. Res. **111:** C08005, doi:10.1029/2005JC003207

VAN LENNING, K., I. PROBERT, M. LATASA, M. ESTRADA, AND J. R. YOUNG. 2004. Pigment diversity of coccolithophores in relation to taxonomy, phylogeny and ecological preferences, p. 51–74. *In* H. R. Thierstein and J. R. Young [eds.], Coccolithophores, from molecular processes to global impact. Springer.

WHITNEY, F. A. 2011. Nutrient variability in the mixed layer of the subarctic Pacific Ocean, 1987–2010. J. Oceanography **67:** 481–492, doi:10.1007/s10872-011-0051-2

WILLIAMS, P. L. B. 1998. The balance of plankton respiration and photosynthesis in the open oceans. Nature **394:** 55–57, doi:10.1038/27878